Contents lists available at ScienceDirect

Heliyon

Comprehensive evaluation of cell death-related genes as novel diagnostic biomarkers for breast cancer

Xiaoyue Shi [a,1], Hao Ding [b,1], Jing Tao [c], Yanhui Zhu [a], Xiaoqiang Zhang [a], Gao He [a], Junzhe Yang [a], Xian Wu [a], Xiaoan Liu [a,**], Xiafei Yu [a,*]

[a] Department of Breast Surgery, The First Affiliated Hospital of Nanjing Medical University, 300 Guangzhou Road, Nanjing, Jiangsu, 210029, People's Republic of China
[b] Department of Breast Surgery, Baoying Maternal and Child Health Hospital, 120 Anyi East Road, Yangzhou, Jiangsu 225800, People's Republic of China
[c] Department of Thyroid-Breast Surgery, Nanjing Pukou Hospital, The Fourth Affiliated Hospital of Nanjing Medical University, 18 Puyuan Road, Nanjing, Jiangsu 210031, People's Republic of China

ARTICLE INFO

ABSTRACT

Background: Breast cancer (BRCA) ranks first among cancers in terms of incidence and mortality rates in women, primarily owing to metastasis, chemo-resistance, and heterogeneity. To predict long-term prognosis and design novel therapies for BRCA, more sensitive markers need to be explored.

Methods: Data from 1089 BRCA patients were downloaded from TCGA database. Pearson's correlation analysis and univariate and multivariate Cox regression analyses were performed to assess the role of cell death-related genes (CDGs) in predicting BRCA prognosis. Kaplan–Meier survival curves were generated to compare the overall survival in the two subgroups. A nomogram was constructed using risk scores based on the five CDGs and other clinicopathological features. CCK-8, EdU incorporation, and colony formation assays were performed to verify the inhibitory effect of NFKBIA on BRCA cell proliferation. Transwell assay, flow cytometry, and immunohistochemistry analyses were performed to ascertain the biological function of NFKBIA.

Results: Five differentially expressed CDGs were detected among 156 CDGs. The risk score for each patient was then calculated based on the expression levels of the five CDGs. Distinct differences in immune infiltration, expression of immune-oncological targets, mutation status, and half-maximal inhibitory concentration values of some targeted drugs were observed between the high- and low-risk groups. Finally, in vitro cell experiments verified that NFKBIA overexpression suppresses the proliferation and migration of BRCA cells.

Conclusions: Our study revealed that some CDGs, especially NFKBIA, could serve as sensitive markers for predicting the prognosis of patients with BRCA and designing more personalized clinical therapies.

* Corresponding author.
** Corresponding author.
   E-mail addresses: liuxiaoan@njmu.edu.cn (X. Liu), 347311312@qq.com (X. Yu).
[1] Xiaoyue Shi and Hao Ding have contributed equally to this work.

List of abbreviations

BRCA	breast cancer
CDGs	cell death-related genes
TCGA	The Cancer Genome Atlas
ROC:	receiver operating characteristic
GO	Gene Ontology terms
KEGG	Kyoto Encyclopedia of Genes and Genomes
GSVA	Gene Set Variation Analysis
IC 50	half maximal inhibitory concentration; oe: overexpression
CCK-8	Cell Counting Kit-8; EdU:5-ethynyl-2′-deoxyuridine;
HER2	human epidermal growth factor 2
ATG	autophagy-related
DRs	death receptors
RCD	regulated cell death
ROS	reactive oxygen species
ER	endoplasmic reticulum
DAMPs	danger-associated molecular patterns
TME	tumour microenvironment
OS	overall survival
MSigDB	Molecular Signatures Database
MF	molecular function
BP	biological process
CC	cellular component
GSEA	gene set enrichment analysis
ssGSEA	single sample gene set enrichment analysis
RIPA	radioimmunoprecipitation assay
SDS–PAGE	10 % sodium sulfate polyacrylamide gel electrophoresis
ECL:	enhanced chemiluminescent
PI	propidium iodide;
HR	hazard ratio
AUC	area under the curve
DEGs	differentially expressed genes
FDR	false discovery rate
FC	fold change
IFNγ	interferon γ
TNF	tumour necrosis factor
RT-qPCR	Quantitative Real-Time PCR
WB	western blotting
EdU	5-ethynyl-2′- deoxyuridine;
CCK8	cell counting kit-8
IHC	immunohistochemistry

1. Introduction

Breast cancer (BRCA) has surpassed lung cancer as the most common cancer in women, with roughly 2.3 million new cases reported annually [1–3]. Owing to the low fertility rate, physical inactivity, and excess body weight, its morbidity is estimated to increase by 0.5 % per year [4]. BRCA can be treated with systemic (endocrine therapy, chemotherapy, targeted therapy, immunotherapy, and gene therapy) and local therapies (surgical resection and postoperative radiation) [5]. However, its prognosis remains poor [6], with 685, 000 deaths worldwide, primarily due to metastasis or chemo-resistance [7]. Therefore, novel biomarkers are required to predict the prognosis of BRCA and design new therapeutic options.

Cell death is indispensable for physiological growth of multicellular organisms. Excessive cell death can eliminate healthy cells from degenerative diseases [8]. In addition, cell death can also be disrupted to generate dysfunctional cells, including those with aberrant DNA, thus initiating the progression of cancer [9,10]. Cell death is primarily achieved through apoptosis, autophagy and necrosis [11]. Autophagy refers to the degradation of cellular macromolecules with lysosomes and the utilization of recycled nutrients to generate energy and alleviate cellular damage [12,13]. Excessive autophagy may induce cellular apoptosis and necrosis of cells [14]. The autophagy machinery involves autophagy-related (ATG) proteins, cytoskeletal components, tumour suppressors, immu-noproteins, and various signalling pathways [15]. Apoptosis is characterized by its separation from the extracellular matrix, chro-mosomal condensation, DNA fragmentation, and plasma membrane blebbing. Additionally, it is either intrinsic (induced by disruption

of intracellular homeostasis) or extrinsic (induced by extracellular signalling involving death receptors) [16]. Necrosis, a stress-related regulated cell death (RCD) induced by environmental perturbations, causes membrane dissolution and loss of cellular content [17]. Colliquative, caseating, liquefactive, and fibrinoid necrosis have been described [18]. The three crucial signalling pathways involved in necrosis are MLKL, RIPK3 and RIPK1 [19]. Pyroptosis and ferroptosis may be activated upon exposure to pathogens or innate stress [20]. All of these mechanisms cooperate to determine the fate of a cell [21].

Aberrant expression of cell death-related genes (CDGs) and pathway activation are associated with tumour malignancy. Autophagy can inhibit the development of cancer in the early stages by suppressing tumour inducers, such as reactive oxygen species (ROS), inflammation, DNA damage, genome instability, and tissue damage [22]. Autophagy then turns oncogenic by adapting cancer cells to stresses (inflammatory, metabolic, and genotoxic) in the tumour microenvironment and increasing their invasiveness [23]. Interactions between autophagy and tumour growth have also been reported. For example, the expression of MIR93 (microRNA-93) influences glioblastoma by inhibiting autophagy regulators such as SQSTM1/p62, ATG5, ATG4B and BECN1/Beclin 1 [24]. Autophagy is repressed in hepatocellular carcinoma [25] but is enhanced in pancreatic ductal adenocarcinoma and cholangiocarcinoma [26,27]. As a tumour suppressor gene, p53 activates many apoptosis-related genes and pathways, including mitochondria-dependent and endoplasmic reticulum (ER) stress-dependent signalling pathways [28].

Molecules that can induce cellular apoptosis may be used to design anticancer treatments, such as melanoma differentiation-associated gene-7 (MDA-7) and interleukin-24 (IL-24) for melanoma [29], and KRAS, EGFR, or ALK inhibitor ALSO for lung cancer [30]. β-Glucan promotes apoptotic death of cancer cells [31]. In contrast, necrosis drives tumorigenesis through different mechanisms. First, danger-associated molecular patterns (DAMPs), including HMGB-, are released to give rise to inflammation, thus accelerating tumour development [32]. Angiogenesis and cell-cell interactions are enhanced in the context of necrosis [33]. RIPK3, a protein involved in the necrosis-related signalling pathway, is upregulated in cervical cancer [34]. However, the role of BRCA in cell death remains unclear.

The tumour microenvironment (TME) contains malignant cells, adipocytes, fibroblasts, tumour vasculature, lymphocytes, dendritic cells, and cancer-associated fibroblasts [35]. Abnormal cell death may distort the composition of immune cells in the TME, thereby influencing tumour progression [36,37]. It has been reported that knockdown of MCT4, which regulates the transport of lactic acid and lactate in the microenvironment, inhibits autophagy and significantly improves the prognosis of patients with bladder cancer [38]. CDGs that activate the adaptive immune response may function as prognostic biomarkers in lower-grade glioma [39]. Several studies have evaluated the profile of cell death-related genes in the TME of BRCA.

In this study, based on The Cancer Genome Atlas (TCGA) dataset, we determined the prognostic value of CDGs in patients with BRCA using bioinformatics and statistical analyses. Five CDGs with strong correlations with the overall survival (OS) of patients with BRCA were selected and used to calculate risk scores. Based on the median risk scores, BRCA patients were classified into low- and high-risk groups. Survival was worse, and the expression levels of tumour biomarkers were higher in the high-risk subgroup. Enrichment analyses were performed to determine the tumorigenic mechanisms of the CDGs. A nomogram model was constructed to predict the OS of BRCA patients with different clinicopathological features. Finally, we validated the role of NFKBIA in BRCA in vitro.

2. Materials and methods

2.1. Data collection

To assess the prognostic value of CDGs in BRCA, data on 156 CDGs in 1089 BRCA patients, the corresponding clinical annotations, and somatic mutation data were retrieved from TCGA database (https://portal.gdc.cancer.gov). For clarity, we divided the 156 CDGs into categories (34 autophagy-related genes, 86 apoptosis-related, and 49 necrosis-related genes) using the AmiGO 2 tool (http://amigo.geneontology.org/amigo/landing). The exact GO IDs used are explicitly listed in Supplementary Table 2, ensuring replicability. During data pre-processing, we first screened the differentially expressed genes (DEGs) between cancer and adjacent normal tissues. We set a strict criterion for DEGs ($|\log2(FC)| > 1$ and $p < 0.05$) to enhance the accuracy of the results. Through machine learning technology, the 1089 patients from the TCGA cohort were randomly divided into a training set and a testing set by using the "caret" R package (https://CRAN.R-project.org/package=corrplot), and the Cox regression analysis was performed. All clinical samples (four pairs of BRCA and paracancerous tissue specimens) were acquired from the First Affiliated Hospital of Nanjing Medical University with informed consent from the patients.

2.2. Construction and assessment of BRCA-related CDGs

First, a Pearson's correlation analysis was performed to select CDGs. We included only those CDGs with | Pearson R | >0.5 and $p < 0.05$ to ensure a robust analysis, thus, we found 5 CDGs that could meet the criteria. Univariate and multivariate Cox regression analyses were applied to the training and validation cohorts to determine the significance of the five prognostic CDGs. The coefficients of the five CDGs were obtained via cross-validation using the R package "glmnet" [40]. Then, the risk score was calculated as follows: risk score = (0.0175 × PIK3CA expression level) + (0.0254 × AIFM1 expression level) + (0.0195 × GABARAPL2 expression level) + (0.1076 × ATG4A expression level) - (0.00996 × NFKBIA expression level). We calculated the risk score for each patient in TCGA cohort. Subsequently, the patients were divided into low- and high-risk subgroups based on median risk scores. GSE1456, available from the Gene-Expression Omnibus (GEO) database (https://www.ncbi.nlm. nih.gov/geo/), involving 159 cases, were used for external validation. GSE7390, GSE16446, GSE20685, GSE20711, GSE42568, GSE45255, GSE4839, and GSE58812 were obtained from the GEO database.

2.3. Differential expression, mutation and functional enrichment analyses

The "limma" R package [41] was used to identify DEGs between the two risk groups based on |log2 (Fold change (FC)) | > 1 and p < 0.05. We also downloaded the gene set including "c2.cp.kegg.v7.1" and "h.all.v7.2" from the Molecular Signatures Database (MSigDB) to conduct GSVA (gene set variation analysis) [42]. The mutation rate was visualized using the R package "maftools" [43]. Enriched GO terms in three aspects (molecular function [MF]), biological process [BP], cellular component [CC]), and the enriched Kyoto Encyclopedia of Genes and Genomes (KEGG) pathways (https://www.kegg.jp) were identified. The R packages "ggplot2" [44], "clusterProfiler" [45], "GOplot" [46] and "enrichplot" [47] were used to obtain enriched results in GO and KEGG analyses.

2.4. Tumour immune cell infiltration and potential therapeutic value of CDGs

Single-sample gene set enrichment analysis (ssGSEA) was performed using the R package "gsva" to quantify the expression levels of 28 immune cell type markers. The "estimate" [48] R package's output was used to investigate the differences in the levels of immune cells between the two groups. The interaction between immuno-oncological targets and CDGs was depicted using the R package "corrplot" [49]. The half-maximal inhibitory concentration (IC50) values of the drugs mentioned previously were downloaded from the CellMiner database (https://discover.nci.nih.gov/cellminer/home.do). The R package "pRRophetic" [50] was used to predict the drug sensitivity.

2.5. Clinical correlation and nomogram construction

Then, univariate and multivariate Cox proportional regression analyses were conducted on the "Survival" and "Survminer" (https://CRAN.R-project.org/package=survminer) R packages to assess the relationship between clinicopathological features (age, stage, tumor size, the presence or absence of regional lymph node spread and PAM50) and OS. Kaplan–Meier survival curves were also plotted to compare OSs between the two subgroups. To show the relationship between the expression of CDGs and clinicopathological features, a heatmap was generated by using the "pheatmap" R package (https://CRAN.R-project.org/package=pheatmap). The "rms" R package [51] was utilized to construct the nomogram based on risk score, age, stage, T, N, and PAM50.

2.6. Cell lines and cultures

The MDA-MB-231 and ZR-75-1 breast cancer cell lines utilized in this research were acquired from the Cell Center of the Shanghai Institutes for Biological Sciences (Shanghai, China). The MDA-MB-231 and ZR-75-1 cells were cultured in a complete growth medium, enriched with 10 % fetal bovine serum (FBS; WISENT, Canada), and maintained in a humidified environment composed of 95 % air and 5 % CO2 at a temperature of 37 °C. The cells were sub-cultured upon reaching an approximate confluence of 70 %.

2.7. Quantitative Real-Time PCR

Total RNA was extracted from BRCA and normal tissues using the TRIzol reagent (Invitrogen, Carlsbad, CA, USA), and cDNA was subsequently synthesized with HiScript II Reverse Transcriptase (Vazyme, Nanjing, China). We executed the real-time quantitative PCR employing Hieff® qPCR SYBR Green Master Mix (Yishen, Shanghai, China). The reaction was set up in a total volume of 20 μL with the following conditions: initial denaturation at 95 °C for 10 min, followed by 40 cycles of denaturation at 95 °C for 15 s, and annealing/extension at 60 °C for 1 min. The $2^{-\Delta\Delta Ct}$ method was employed to analyze the relative mRNA expression levels. Each sample underwent triplicate detection. The primer sequences were as follows: NFKBIA forward primer:5′ CTCCGAGACTTTCGAGGAAATAC 3′, reverse primer:5′ GCCATTGTAGTTGGTAGCCTTCA 3'.

2.8. Transfection

The plasmid utilized in this research was acquired from Heyuan Biology Technology Co., Ltd (Shanghai, China). According to the guidelines provided by the manufacturers, the pcDNA plasmids underwent transfection utilizing linear polyethylenimine (PEI) MW40000 from Yeasen Biotechnology Co., Ltd. (Shanghai, China).

2.9. Western blotting assay

Total protein was extracted from BRCA cells using radioimmunoprecipitation assay (RIPA) lysis buffer (Beyotime, China), loaded onto 10 % sodium sulfate polyacrylamide gel electrophoresis (SDS–PAGE) gels, and transferred to 0.22 μm PVDF membranes (Millipore, USA). After blocking with 5 % nonfat milk powder for at least 1 h at room temperature, the membranes were incubated overnight with primary antibodies (Anti-IKB alpha antibody, Abcam, ab76429, Dilutions 1:1000) at 4 °C on a rotator, incubated with the appropriate secondary antibodies (HRP Goat Anti-Rabbit IgG, ABclonal, AS014, Dilutions 1:10000), and shaken at room temperature for 1 h. Protein bands were visualized using an enhanced chemiluminescence (ECL) system (Bio-Rad, Hercules, CA, USA). The α-tubulin was considered as an internal control.

2.10. EdU incorporation assay

The MDA-MB-231 and ZR-75-1 BRCA cells were respectively plated in 96-well plates (5×10^4 cells/well) 24 h post-transfection. Cell proliferation was assessed utilizing a 5-ethynyl-2′-deoxyuridine (EdU) incorporation assay kit (RiboBio, China). Subsequently, cell nuclei were stained with 100 μL of Hoechst 33342 (5 μg/mL) for a duration of 30 min, and visualizations were obtained using a fluorescence microscope (Leica, Germany).

2.11. CCK-8 assay

During the study, a Cell Counting Kit-8 (CCK-8, Beyotime, China) was utilized. The MDA-MB-231 and ZR-75-1 BRCA cell suspensions were individually arranged in a 96-well plate at a density of 2×10^3/well in 200 μL of medium, 24 h post-transfection. These were then pre-incubated at 37 °C for 24 h in an incubator. Subsequently, 10 μL of the test substance was incorporated into the culture plate, followed by a 4-day incubation period. Afterwards, CCK-8 solution was dispensed into each well and a further incubation of 2 h was conducted. The optical density at 450 nm was ascertained using a microplate reader (Dojindo Molecular Technologies, Kumamoto, Japan).

2.12. Colony formation assay

The MDA-MB-231 and ZR-75-1 BRCA cells were seeded in 6-well plates (600 cells/well) and cultured at 37 °C and 5 % CO2 for 14 days. The cell colonies were then fixed with 4 % paraformaldehyde, and stained with 0.1 % crystal violet (Beyotime, Shanghai) for 30 min. Cell colonies were imaged using a digital camera and manually counted.

2.13. Cell apoptosis assay

The MDA-MB-231 and ZR-75-1 BRCA cells (1×10^5 cells/well) were cultured in 6-well plates, washed with PBS, and collected by adding trypsin cell digestion solution. Next, the cells were resuspended in 500 μl of binding buffer. One hour after incubation with 5 μl of Annexin V-FITC and 5 μl of propidium iodide (PI) (BD Biosciences, USA) at room temperature for 10 min in the dark, the cells were examined using a FACSCalibur (BD Biosciences, USA).

2.14. Cell cycle analysis

The MDA-MB-231 and ZR-75-1 BRCA cells in the logarithmic growth phase were first inoculated (2 mL) into 6-well plates at 1×10^6 cells/mL, cultured, collected, washed twice with precooled PBS, and fixed with pre-cooled 75 % ethanol at 4 °C for more than 4 h. After the cells were incubated with 400 μL propidium iodide (PI, 50 μg/mL) and 100 μL RNase A (100 μg/mL) at 4 °C for 30 min in the dark, the cells were counted using a flow cytometer (FACS Calibur, BD Biosciences, USA). The results were analysed using FlowJo software.

2.15. Transwell assay

Transwell chambers (pore size 8 μm; Millipore, USA) with (transwell invasion assay) or without (transwell migration assay) 10 μg Matrigel (BD Biosciences, USA) were used to perform the Transwell assay. A total of 3×10^4 MDA-MB-231 or ZR-75-1 BRCA cells were plated in the upper insert of the Transwell chamber with serum-free medium, and 600 μL of medium containing 15 % FBS was added to the lower chamber. After incubation for 24h at 37 °C, the non-migrated cells on the upper surface of the chamber were wiped off and the cells on the bottom surface of the chamber were washed twice with calcium-free PBS, fixed with 4 % formaldehyde for 30 min, and stained with 0.1 % crystal violet for 10 min (Beyotime, China). Cells were observed and counted by an inverted microscope.

2.16. Immunohistochemistry analysis

Sections of BRCA and normal tissues were paraffin-embedded, dewaxed with xylene and ethanol at various concentrations (75 %, 80 %, 90 %, 95 %, and 100 %), and antigen-retrieved with sodium citrate buffer (Beyotime, China) at 98 °C at double boiler for 30 min. Endogenous peroxidase blocking buffer and immunol staining blocking buffer (Beyotime, China) were used for inactivation of endogenous peroxidase and serum blockade, respectively. Afterwards, the sections were incubated with IkB Alpha Polyclonal antibody (Proteintech; cat no. 10268-1-AP; Dilution 1:200) or AIF Polyclonal antibody (Proteintech; cat no. 17984-1-AP; Dilution 1:200) overnight at 4 °C, and then incubated with HRP-polymer-conjugated secondary antibody (Abcam, UK) for 1h at RT. Finally, 3,3′-diaminobenzidine (DAB) (MXB, China) and hematoxylin and eosin (Beyotime, China) were used to stain the sections, which were then observed under a microscope (Olympus, Japan). The IHC results were quantified using Image J.

2.17. Statistical analysis

All statistical analyses were performed using R software (version 4.0.1). Statistical significance was set at P < 0.05. Student's t-test was used to compare the expression of immune-oncological targets and gene mutations in the two subgroups. Pearson's correlation test

was performed to analyze the correlation between CDG expression and immune infiltration. Pearson's chi-squared ($\chi 2$) test was used to assess the association between CDG expression and clinicopathological features. We also applied univariate and multivariate Cox regression analyses to evaluate the significance of CDGs in predicting BRCA prognosis. We established a nomogram using the factors from the multivariate Cox regression analysis to predict 3.5-, 5-, and 7.5-year survival rates, and the accuracy of the nomogram was verified using calibration plots. The predictive value of the CDGs was estimated using the receiver operating characteristic (ROC) curves and area under the curve (AUC) values, and the "pROC" R package [52] was used to quantify the AUC values.

3. Results

3.1. Identification of CDGs in BRCA patients

A total of 156 CDGs were screened from TCGA dataset, including 34 autophagy-related genes, 86 apoptosis-related genes, and 49 necrosis-related genes. Their expression data in tumour-adjacent normal tissues and BRCA tissues were collected from 1089 patients in TCGA cohort (Fig. S1). Gene expression was different among the 111 CDGs ($p < 0.05$). In a 1:1 ratio, 1089 patients with BRCA were randomly assigned to a training cohort (n = 545) and a validation cohort (n = 544). Using univariate and multivariate Cox regression analyses, we discovered that five genes (NFKBIA, PIK3CA, AIFM1, GABARAPL2, and ATG4A) were most significantly associated with BRCA risk and could be used to calculate the risk scores. The flowchart of the study is shown in Fig. 1A. Among these genes, we defined NFKBIA as a protective factor, with a hazard ratio (HR) value < 1 (0.986), and the remaining four genes as risk factors, with HR values
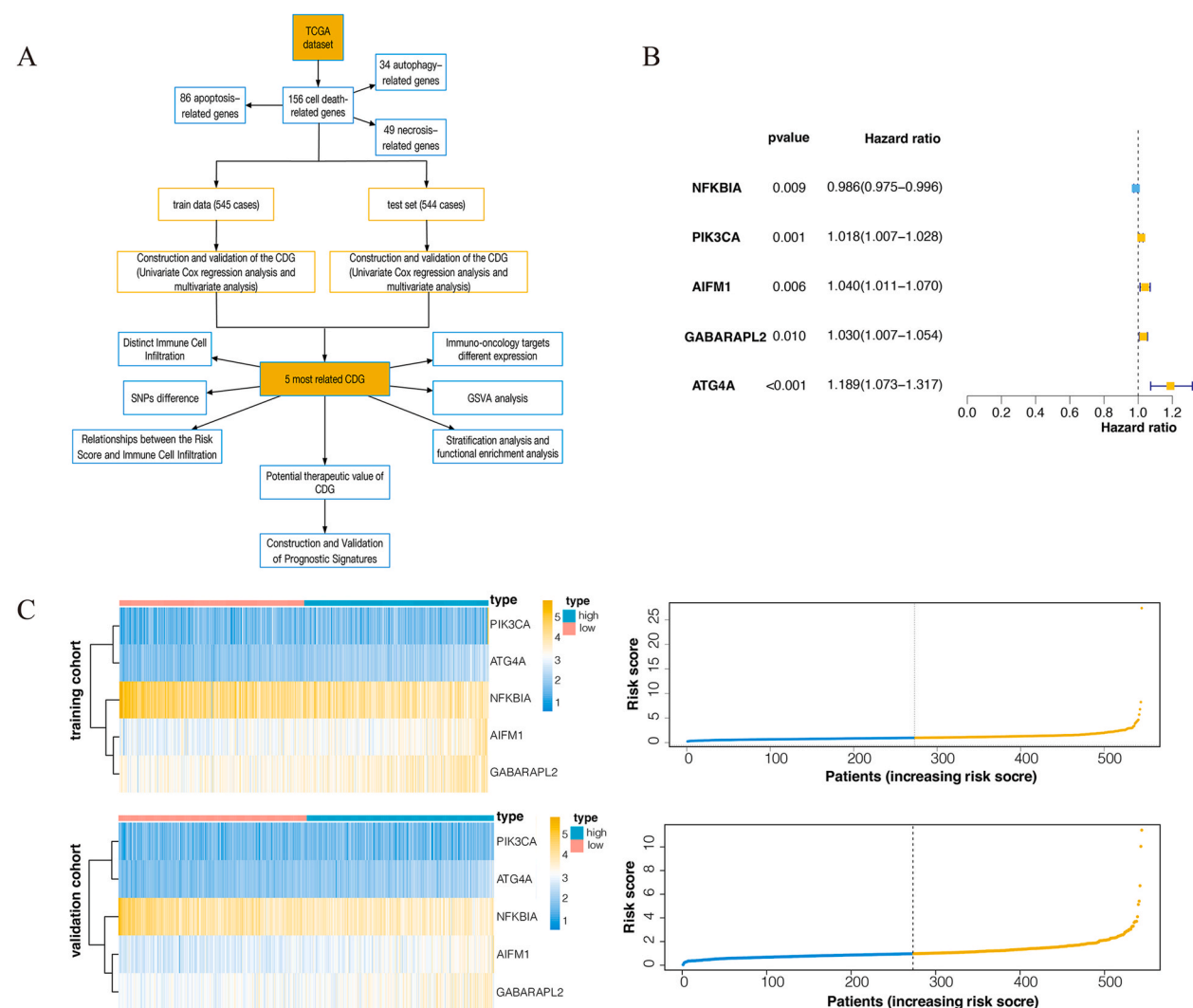
Fig. 1. Identification of CDGs in BRCA patients. (A) Study flowchart. (B) The forest plot of CDGs associated with prognosis and their hazard ratios. (C) Heatmap of the correlations between the expression levels of 5 CDGs and risk scores in the TCGA training and validation cohorts. Risk scores of patients and the median risk score in the two cohorts.

> 1 (1.018, 1.040, 1.030, and 1.189) (Fig. 1B). And the calculation for the risk score was performed using the following formula: risk score = (0.0175 × PIK3CA expression level) + (0.0254 × AIFM1 expression level) + (0.0195 × GABARAPL2 expression level) + (0.1076 × ATG4A expression level) - (0.00996 × NFKBIA expression level). Each patient in the TCGA cohort had their risk score computed. Following this, patients were segregated into two subgroups of high and low risk based on the median of the calculated risk scores. The heatmap (Fig. 1C) indicated that the expression levels of PIK3CA, AIFM1, GABARAPL2, and ATG4A were upregulated in the high-risk group and NFKBIA in the low-risk subgroup.

3.2. Identification and validation of CDGs in the TCGA cohort

We investigated the prognostic value of CDGs in patients with BRCA. The risk score for each patient was calculated using the
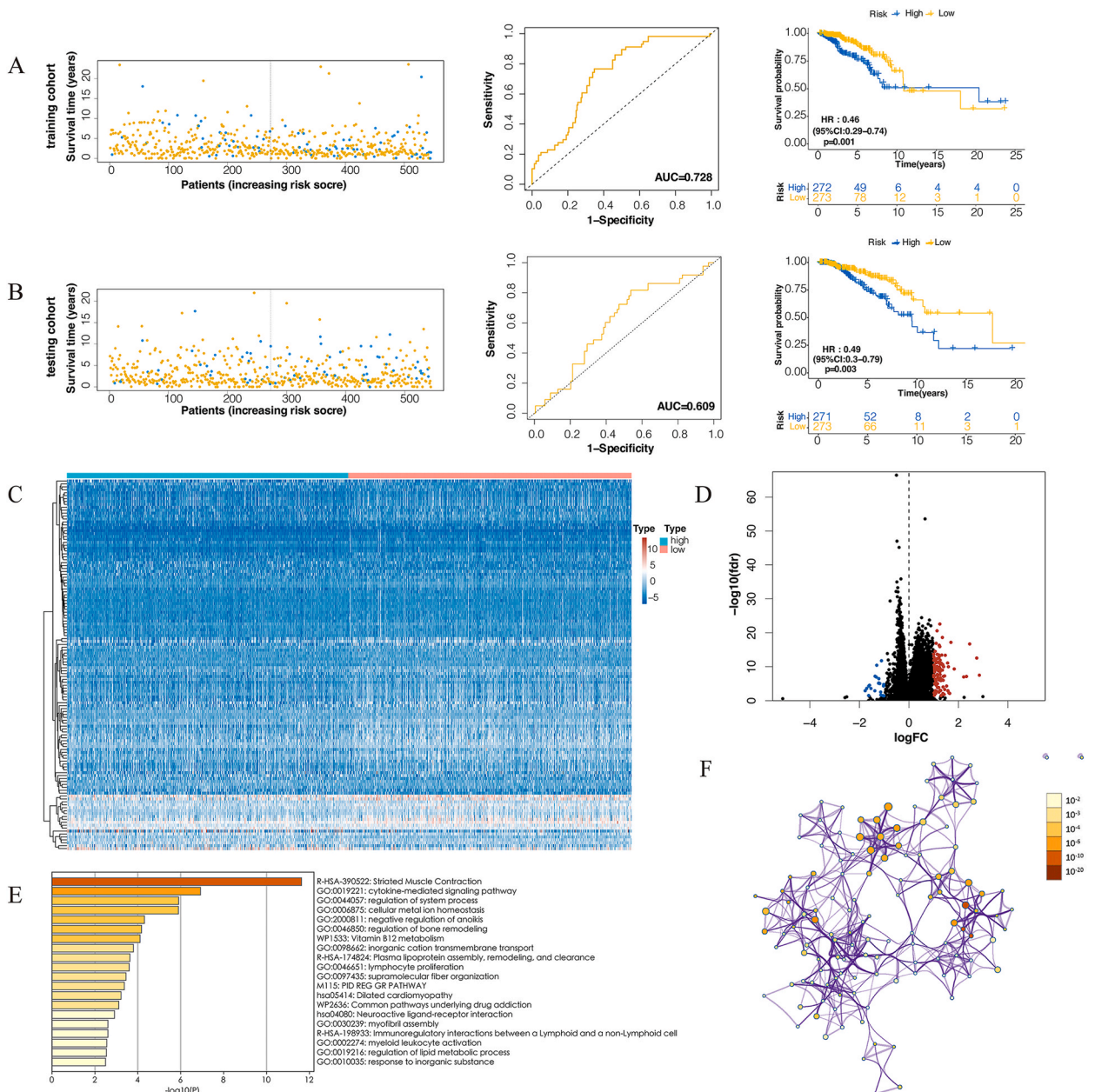
Fig. 2. Identification and validation of CDGs in the TCGA cohort. DEGs and protein-protein interaction enrichment analysis. Distribution of survival status, the ROC curves and the Kaplan–Meier curves of OS for BRCA patients in the TCGA training cohort (A) and validation cohort (B). (C) Heatmap of the correlations between gene expression and risk scores. (D) The volcano plot of DEGs. (E) The GO and the KEGG pathway enrichment analyses for the DEGs. (F) Protein–protein interaction enrichment analysis.
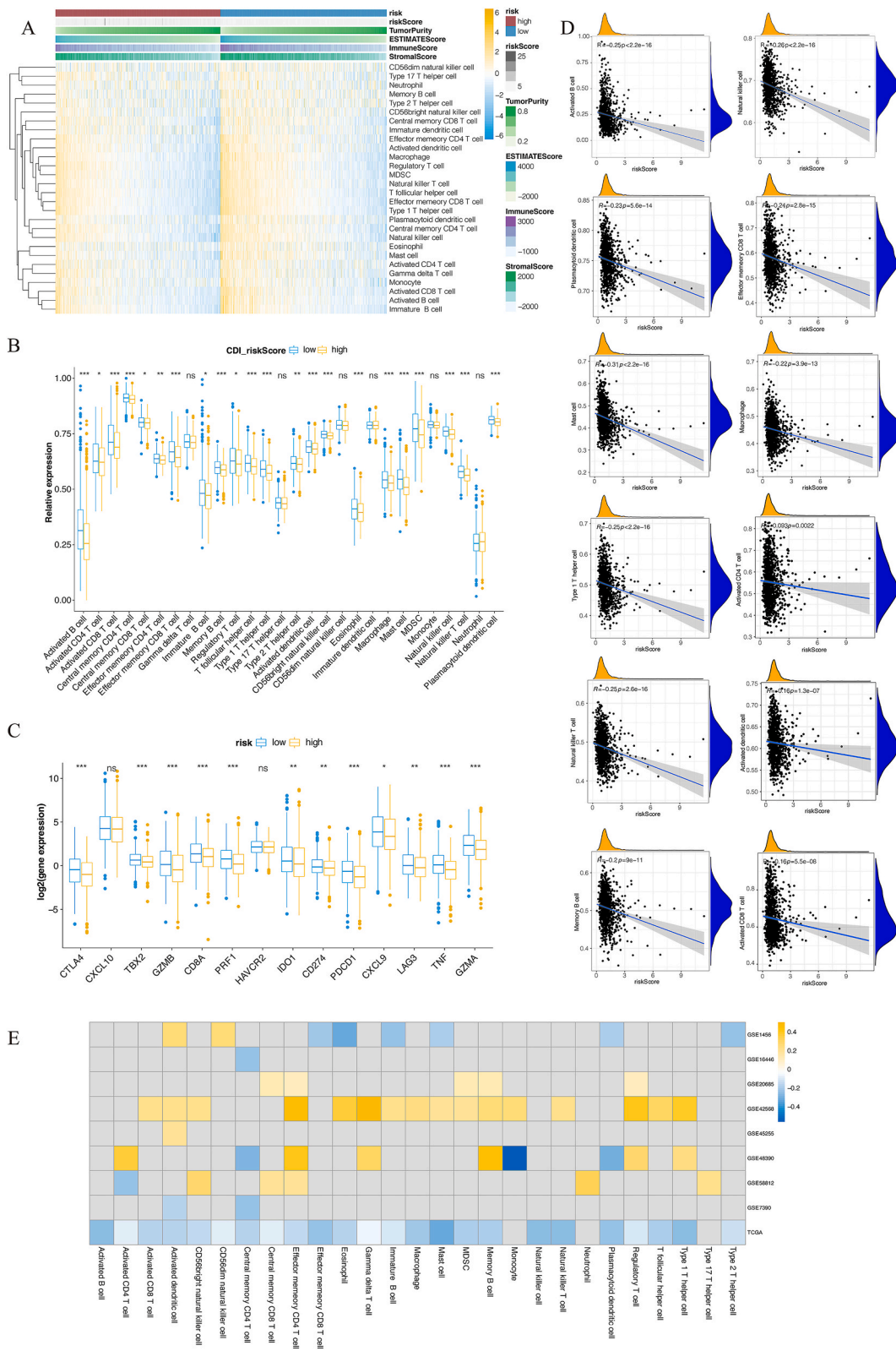
Fig. 3. Interactions of CDGs with immune cells and immune targets. (A) Heatmap of correlations between 28 immune cell types, ESTIMATE scores, immune scores and stromal scores and risk scores. (B) The infiltration levels of 28 immune cell types in the high- and low-risk groups. ns p > 0.05, *p < 0.05, **p < 0.01 and ***p < 0.001. (C) The expression levels of 14 immune targets in the high- and low-risk groups. ns p > 0.05, *p < 0.05, **p < 0.01 and ***p < 0.001. (D) Association between several immune cell types and risk scores. (E) The association between immune cell infiltration and risk score in nine additional datasets.

coefficients obtained based on the expression levels of the five CDGs. The distribution of survival times in the training and validation cohorts is plotted. The AUC value of the five-CDG signature was 0.728 and 0.609 in the training and validation cohorts, respectively. The Kaplan–Meier survival curves showed that the high-risk group had worse survival (lower survival probability and shorter survival time), with p = 0.001 in the training cohort and p = 0.003 in the testing cohort (Fig. 2A and B).

3.3. DEGs and protein-protein interaction enrichment analysis

A total of 127 DEGs between the high- and low-risk groups were identified according to a false discovery rate (FDR) value < 0.05 and | Log2 (FC) | >1 (Fig. 2C) and displayed by the volcano plot (Fig. 2D), including 106 downregulated in the low-risk group and 21 upregulated in the high-risk group. In addition, we identified enriched GO terms and KEGG pathways to investigate the possible mechanisms of DEGs. The results of the protein-protein interaction enrichment analyses are shown in Fig. 2F. In GO terms, the DEGs were mainly correlated with cytokine-mediated signalling pathways, regulation of system processes, and cellular metal ion homeostasis (Fig. 2E). KEGG pathway analysis suggested that the DEGs were associated with striated muscle contraction, vitamin B12 metabolism, and the PID REG GR pathway (Fig. 2E).

3.4. Interactions of CDGs with immune cells and immune targets

To investigate the performance of CDGs in the tumour immune microenvironment (TIME), we compared the immune infiltration levels between high- and low-risk groups. The heatmap (Fig. 3A) shows distinct differences in immune infiltration, ESTIMATE score, immune score, and stromal score between the two groups. As shown in Fig. 3B, the low-risk group presented higher infiltration levels of activated B cells, activated CD8 T cells, central memory CD4 T cells, effector memory CD8 T cells, memory B cells, T follicular helper cells, type 1 T helper cells, activated dendritic cells, CD56bright natural killer cells, eosinophils, macrophages, mast cells, MDSCs, natural killer cells, natural killer T cells, and plasmacytoid dendritic cells (all p < 0.001 and |Pearson's R| > 0.2). In addition, a low risk of BRCA was associated with the infiltration of effector memory CD4 T cells, type 2 T helper cells, activated CD4 T cells, central memory CD8 T cells, immature B cells, and regulatory T cells (all p < 0.05). No immune cell type was found in the high-risk group. The remaining six immune cell types showed no differences in infiltration or expression between the risk groups. The low-risk subgroup had higher immune scores than those of the high-risk subgroup. We assessed the interaction between immuno-oncology targets and CDGs by comparing their expression levels in the high- and low-risk groups. The expression levels of CTLA4, TBX2, GZMB, CD8A, PRF1, PDCD1, TNF-, and GZMA were upregulated in the low-risk group (p < 0.001). High expression levels of IDO1, CD274, LAG3 (p < 0.01), and CXCL9 (p < 0.05) were associated with low risk (Fig. 3C). As shown in Fig. 3D, the expression levels of markers for nine immune cell types, including activated B cells, effector memory CD8 + T cells, macrophages, mast cells, memory B cells, natural killer cells, natural killer T cells, plasmacytoid dendritic cells, and type 1 T helper cells, were significantly correlated with the risk score (p < 0.05, |Pearson R| >0.2). We also analysed the association between immune cell infiltration and risk score in nine additional datasets. The heatmap shows consistent correlations (Pearson's R values, P < 0.05) across the datasets (Fig. 3E). Notably, the expression of central memory CD4 T cells exhibited a downwards trend as the risk score increased in GSE7390 (p = 0.0014 and Pearson's R = −0.23), GSE16446 (p = 0.011 and Pearson's R = −0.23), and GSE48390 (p = 0.012 and Pearson's R = −0.28) (Supplementary fig. 4B, 4C and 6A). The associations between the infiltration of several immune cell types and the risk score in the nine additional datasets are displayed in Supplementary figs. 4–6.

3.5. Mutations and GSVA enrichment analysis

Seven genes, including TP53 (32 %), PIK3CA (31 %), TTN (16 %), and GATA3 (11 %), had higher mutation rates than the other genes among the 418 genes altered (84.1 % of all 497 samples) in the high-risk group (Fig. 4A). In the low-risk group, five genes had higher mutation rates than the other genes among the 409 genes altered (85.92 % of all 476 samples). PIK3CA, TP53, CDH1, TTN, and MUC4 had mutation rates of 35, 32, 18, 16, and 10 %, respectively (Fig. 4A). Mutation profiles are shown in Fig. 4B. Next, we performed GSVA (Fig. 4C). A total of 101 KEGG pathways were significantly differentially enriched between the groups. The high-risk group was markedly enriched in homologous recombination and mismatch repair. The low-risk group was enriched in the Notch, JAK-STAT, and B-cell receptor signalling pathways.

3.6. Therapeutic value of CDGs

We evaluated the correlation between the IC50 of the drugs and the expression levels of CDGs. A total of 310 CDG-drug pairs were identified. NFKBIA was associated with resistance to 15 drugs, including the pan-RAF inhibitor TAK−632 (Rs = −0.550, p < 0.001), RAF inhibitor PLX−8394 (Rs = −0.490, p < 0.001), dabrafenib (Rs = −0.511, p < 0.001), SB−590885 (Rs = −0.461, p < 0.001),
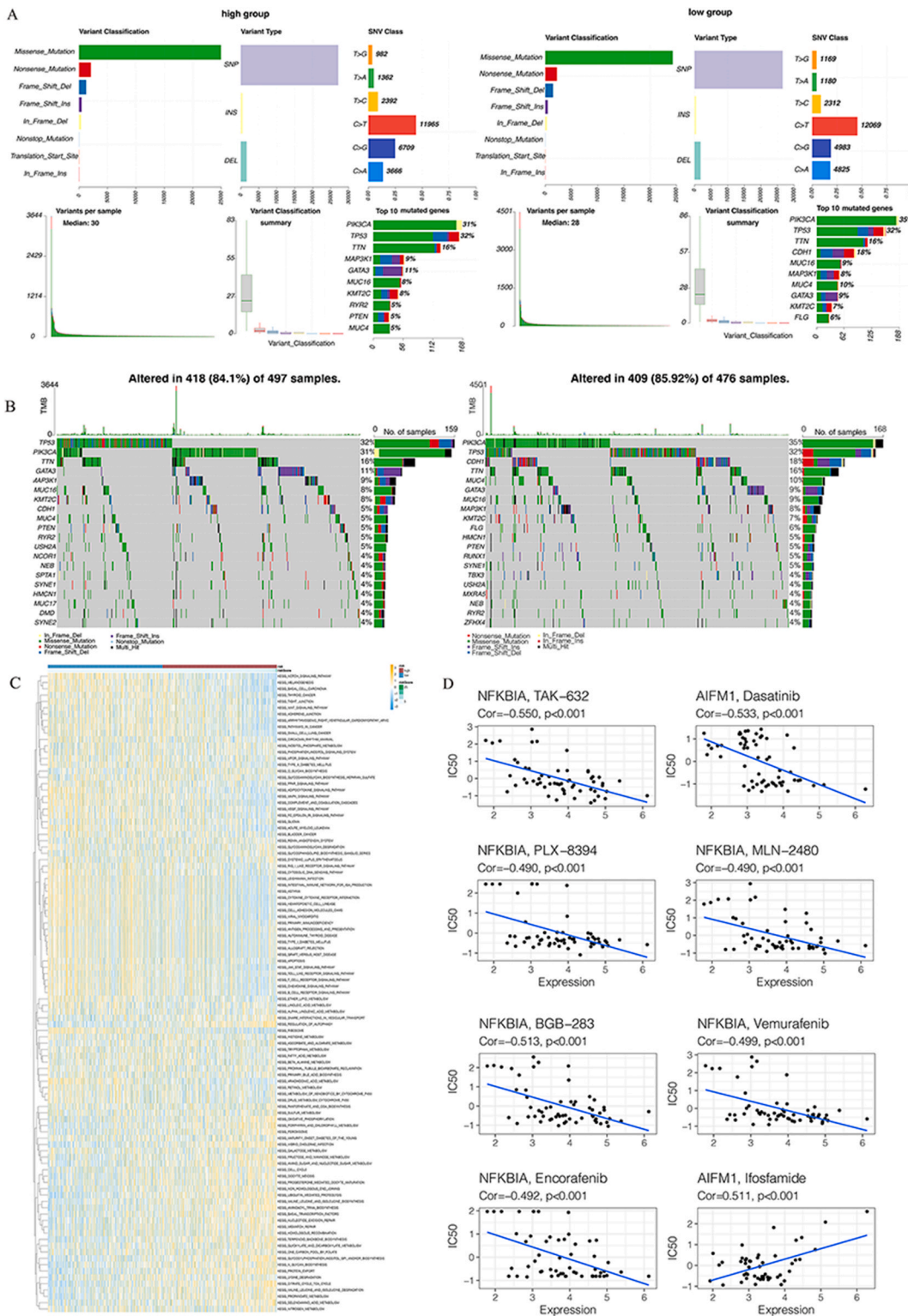
Fig. 4. Mutations and GSVA enrichment analysis as well as the therapeutic value of CDGs. (A) Mutation classification, mutation type, SNV class and top 10 mutated genes in the high/low-risk groups. (B) Waterfall maps of 20 mutated genes in the high- and low-risk groups. (C) Heatmap of the GSVA enrichment results in the high/low-risk groups. (D) Correlations between the IC50 values of eight drugs and the expression levels of CDGs.

LY−3009120 (Rs = −0.444, p < 0.001), encorafenib (Rs = −0.492, p < 0.001), PLX−4720 (Rs = −0.441, p < 0.001), vemurafenib (Rs = −0.499, p < 0.001), ARQ−680 (Rs = −0.464, p < 0.001), MEK inhibitor PD 184352 (Rs = −0.448, p < 0.001), COX inhibitor MLN−2480 (Rs = −0.490, p < 0.001), RAF and EGFR inhibitor BGB−283 (Rs = −0.513, p < 0.001), Abl-Lyn inhibitor Bafetinib (Rs = −0.464, p < 0.001) and ERK inhibitor GDC−0994 (Rs = −0.437, p < 0.001). AIFM1 expression correlated with the response to the tyrosine kinase receptor inhibitor dasatinib (Rs = −0.533, p < 0.001) and the DNA/RNA synthesis inhibitor ifosfamide (Rs = 0.511, p
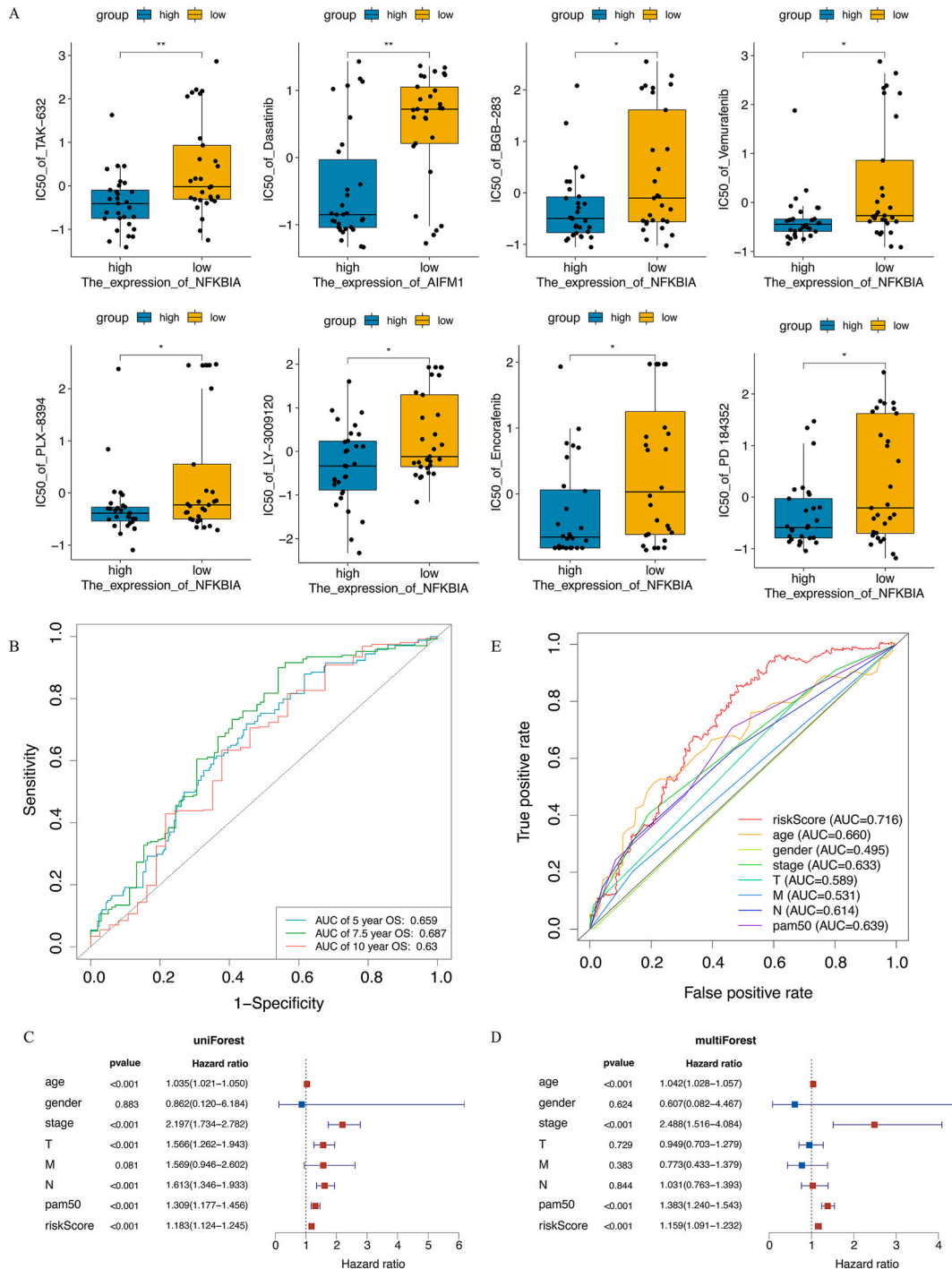
Fig. 5. Stratification analysis and prognostic values of CDGs. (A) The IC50 values of 8 drugs in the high/low-expression groups. (B) The ROC curves for 5-, 7.5- and 10-year OS. (C, D) The risk score was an independent prognostic predictor according to univariate and multivariate analyses. (E) ROC curves for the risk score, age, sex, stage, TNM stage and PAM50.

< 0.001) (Fig. 4D and Supplementary Fig. 2A). Furthermore, BRCA patients were divided into high- and low-expression subgroups based on the median expression levels of two CDGs, NFKBIA and AIFM1. Fig. 5A demonstrates the difference in IC50 between the high- and low-expression groups. The IC50 values of TAK−632, PLX−8394, PD 184352, LY−3009120, BGB−283, encorafenib, and vemurafenib were upregulated in the low NFKBIA expression subgroup. The IC50 value of dasatinib was higher in the low AIF-M1expression group. Therefore, the expression levels of CDGs could be used to predict the effects of treatment.

3.7. Stratification analysis and prognostic values of CDGs

We conducted ROC analysis of the 5-, 7.5-, and 10-year OSs (Fig. 5B). The AUC values (0.659, 0.687, and 0.63, respectively) demonstrated that the risk scores of the five CDGs were accurate in forecasting the OS of BRCA. In univariate Cox regression analysis, the risk score based on CDGs was significantly associated with OS (hazard ratio: HR 1.183, 95 % CI:1.124–1.245, p < 0.001) (Fig. 5C). Other clinicopathological features related to OS were age, stage, tumour size, presence or absence of regional lymph node metastasis, and PAM50. In the multivariate Cox proportional regression analysis, only four features were associated with OS: age (hazard ratio [HR] 1.042, 95 % confidence interval [CI]1.028–1.057, p < 0.01), stage (HR 2.488, 95 % CI1.516–4.084, p < 0.001), PAM50 (HR
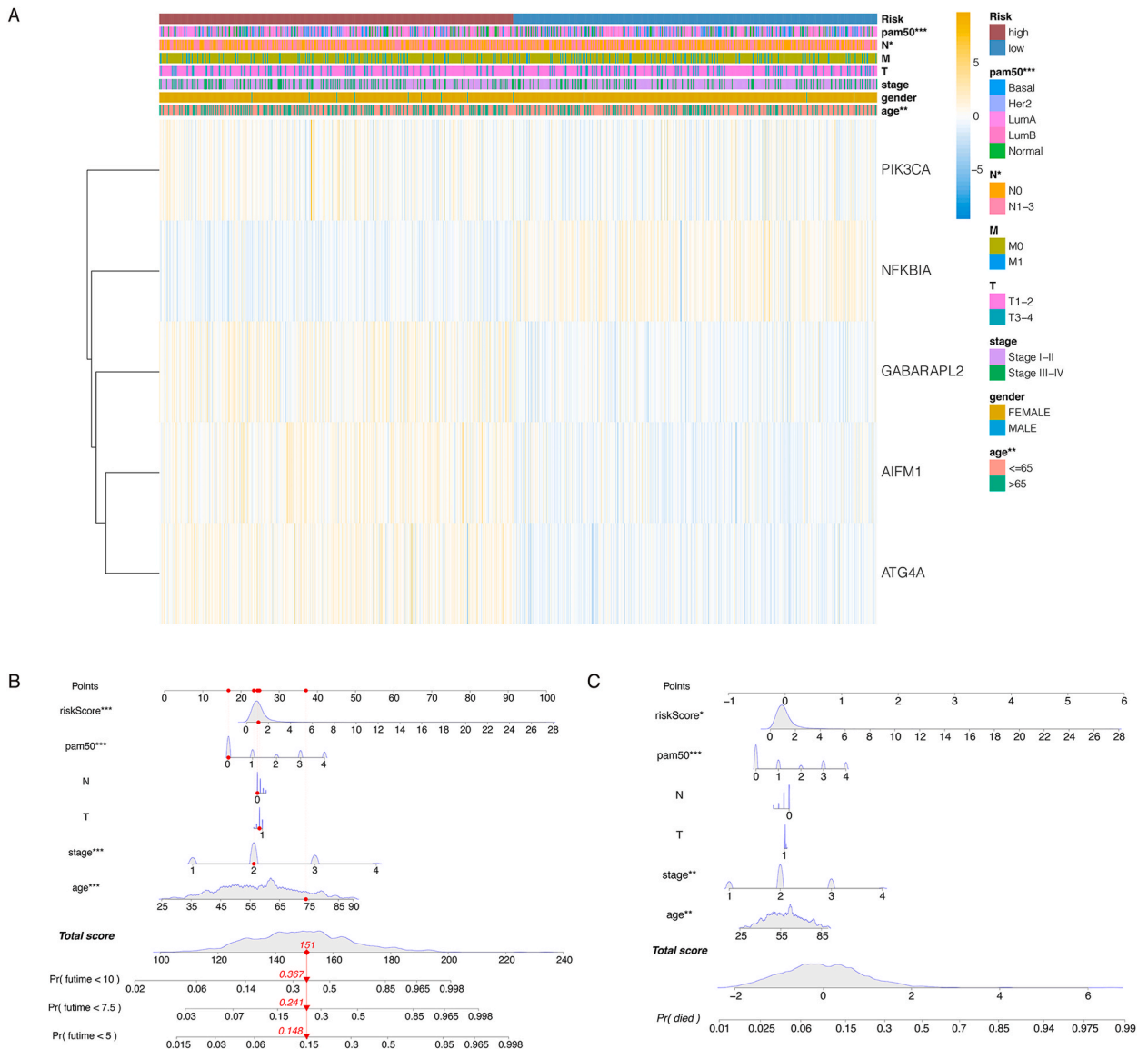
Fig. 6. Construction of the CDG-based nomogram. (A) Heatmap of the correlation between the expression levels of 5 CDGs and risk scores or clinicopathological features. (B, C) The survival (death) rates predicted by the nomogram based on risk score, age, stage, T, N and PAM50 (PAM50: LumA: 0, LumB: 1, Her2: 2, Basal: 3, Normal: 4; T1-2: 0, T3-4: 1; N0: 0, N1-3: 1; Stage I&II: 0, Stage III&IV: 1; age ≤ 65: 0, age>65: 1).

1.383, 95 % CI1.240–1.543, p < 0.01), and risk score (HR 1.159, 95 % CI1.091–1.232, p < 0.001) (Fig. 5D). The AUC values for risk scores, age, sex, stage, T stage, M stage, N stage, and PAM50 in predicting OS were 0.716, 0.660, 0.495, 0.633, 0.589, 0.531, 0.614, and 0.639, respectively (Fig. 5E). The expression levels of PIK3CA, AIFM1, GABARAPL2, and ATG4A were up-regulated in the high-risk group. In contrast, NFKBIA was highly expressed in the low-risk subgroup (Fig. 6A). Their expression levels were also associated with clinicopathological features including sex, age, stage, TNM stage, and PAM50.
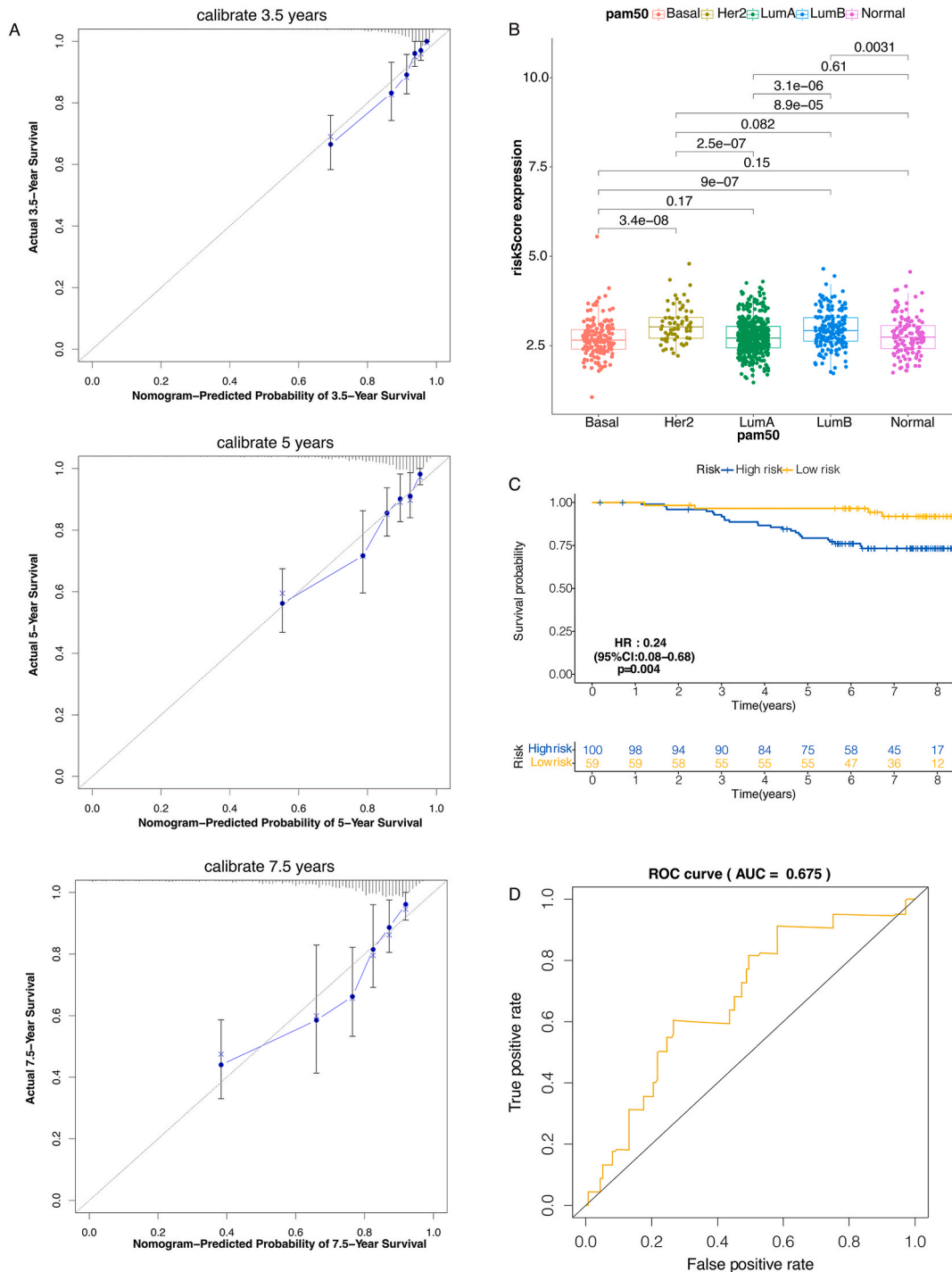
Fig. 7. External validation of the 5 CDGs. (A) Calibration plots of the nomogram for predicting the probability of OS at 3, 5, and 7.5 years. (B) Differences in the risk score between patients grouped according to PAM50. (C) Kaplan–Meier curves of OSs for BRCA patients in the external validation cohort: GSE1456. (D) ROC curve for 5 CDGs in the GSE1456 cohort.
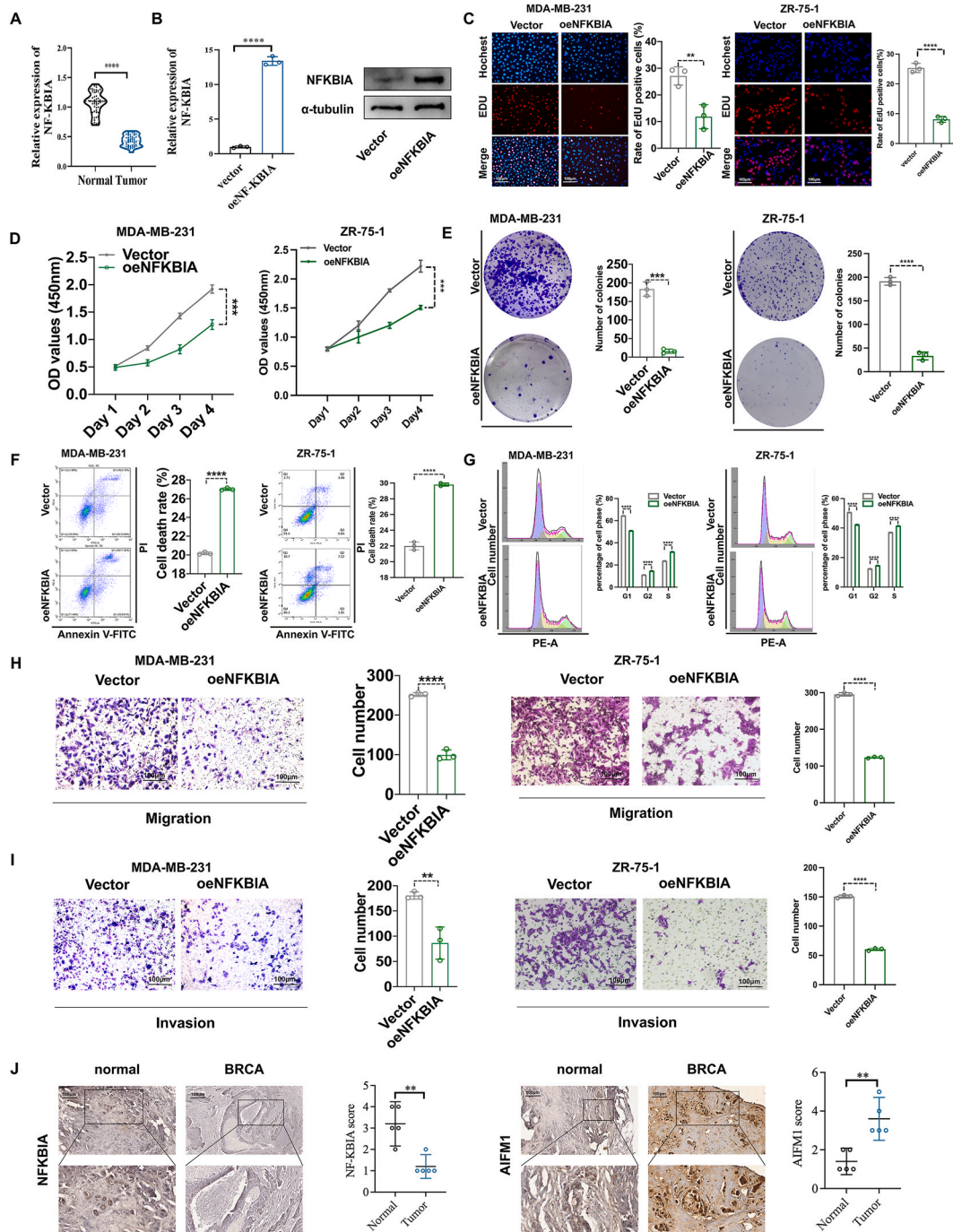
Fig. 8. In vitro cell experiments to explore the biological function of NFKBIA. (A) Expression levels of NFKBIA mRNA in BRCA and normal tissues by RT-qPCR. (B) RT-qPCR and WB to confirm the efficiency of oeNFKBIA. (C) EdU assay was performed to detect the proliferative capacity of the MDA-MB-231 and ZR-75-1 BRCA cells after NFKBIA overexpression. (D) CCK-8 assay was used to examine the proliferation of MDA-MB-231 and ZR-75-1 BRCA cells. (E) Colony formation assay was used to detect the effect of oeNFKBIA on the proliferative ability of MDA-MB-231 and ZR-75-1 cells. (F) Flow cytometry was applied to detect the apoptosis of MDA-MB-231 and ZR-75-1 cells. (G) Cell cycle analysis was applied to count the cells in every phase of the cell cycle. (H, I) Transwell assay was used to determine the migration and invasion of MDA-MB-231 and ZR-75-1 BRCA cells transfected with oeNFKBIA or NC. (J) IHC staining of NFKBIA and AIFM1 in 4 pairs of BRCA and adjacent normal samples.

3.8. Construction of the CDG-based nomogram

We established a nomogram based on CDGs and other clinicopathological features, including age, stage, TNM stage, and PAM50, to predict 3.5-, 5-, and 7.5-year survival rates (Fig. 6B and C). The calibration plots showed perfect consistency between the actual OSs and nomogram-predicted 3.5-, 5-, and 7.5-year survival rates in TCGA cohort (Fig. 7A). Subsequently, we found that the risk score increased distinctly in patients aged >65 years compared with that in younger patients. Patients with tumours that had spread to the lymph nodes (N1-3) tended to exhibit higher risk scores. The risk score was significantly different among the five molecular types of PAM50 (Fig. 7B). Patients with HER2-enriched BRCA had the highest risk score, followed by those with luminal B BRCA and basal-like subtypes. In the GSE1456 and GSE20711 datasets, patients with the basal-like subtype exhibited the highest risk scores (Supplementary Figs. 7A and 8B). Kaplan–Meier curves also demonstrated that high-risk BRCA patients with the following clinicopathological features (age ≤65 years, age >65 years, female sex, T1–2, M0, M1, N0, N1–3, normal subtype, stage I–II) had a longer survival time than low-risk patients (Supplementary Fig. 2B). Kaplan–−Meier curves showed the survival probability of patients with high- or low-risk scores in five different molecular subtypes (Supplementary Fig. 3A). The correlations of risk scores with different clinical features (molecular subtype, surgery type, grade, ER/PR/HER-2 status, and TNM stage) were also presented in patients from nine additional datasets (Supplementary Figs. 7–9).

3.9. External validation of the 5 CDGs

We validated the prognostic value of CDGs using an external cohort (GSE1456 database) of 159 patients with BRCA. In the GSE1456 cohort, the Kaplan–Meier survival curve (Fig. 7C) showed that BRCA patients in the high-risk group had worse survival (lower survival probability and shorter survival time) (p = 0.004). The AUC value for the five-CDG signature in the GSE1456 cohort was 0.676 (Fig. 7D). Similar results were observed in patients from GSE16446 (p = 0.038) (Supplementary Fig. 7C). These findings were in perfect agreement with the TCGA cohort results.

3.10. NFKBIA overexpression suppressed the migration and invasion of BRCA cells

Quantitative Real-Time PCR (RT-qPCR) confirmed that the mRNA levels of NFKBIA were remarkably lower in BRCA tissues than in paracancerous tissues (Fig. 8A). To uncover the biological function of NFKBIA in BRCA cells, we overexpressed NFKBIA using plasmids, the efficiency of which was confirmed by RT-qPCR and Western blotting (Fig. 8B). EdU incorporation (Fig. 8C) and CCK-8 (Fig. 8D) assays confirmed the negative effect of NFKBIA overexpression (oeNFKBIA) on the proliferation of MDA-MB-231 and ZR-75-1 BRCA cells. The colony formation assay showed that the proliferation of MDA-MB-231 and ZR-75-1 BRCA cells was significantly suppressed in the oeNFKBIA group (Fig. 8E). The cell apoptosis assay showed that NFKBIA overexpression increased the apoptosis rate of MDA-MB-231 and ZR-75-1 cells (Fig. 8F). The cell cycle assay (Fig. 8G) showed that oeNFKBIA arrested the cell cycle in G2 and S phases. The Transwell assay strongly indicated that oeNFKBIA attenuated the migration (Fig. 8H) and invasion (Fig. 8I) of two kinds of BRCA cells. Finally, IHC analysis (Fig. 8J) demonstrated that NFKBIA expression was notably lower in BRCA tissues than that in normal tissues. The expression of AIFM1 showed an opposite pattern.

4. Discussion

In the present study, we explored five CDGs that were significantly associated with BRCA development using bioinformatics tools. Among the five CDGs, NFKBIA was significantly downregulated and PIK3CA, AIFM1, GABARAPL2, and ATG4A were upregulated in BRCA tissues. The risk score calculated based on the five CDGs accurately predicted the survival of patients with BRCA. Specifically, the regulatory role of NFKBIA in BRCA development was verified through cellular experiments.

NFKBIA, which is upregulated by circ-CEP85L by sponging miR-942-5p, inhibits gastric cancer progression and invasion [53]. PIK3CA fulfils its oncogenic role by inducing the expression of specific genes in cancers of various cellular origins and molecular phenotypes. For example, PIK3CA induces the lincRNA Neat 1 and the transcription factor Runx 2 to regulate signal transduction, cellular metabolism, and cell adhesion in BRCA [54]. AIFM1 is downregulated by miR-425-5p to increase the viability of cervical cancer cells [55]. GABARAPL2 and ATG4A function as prognostic markers for gastric cancer and BRCA, respectively, and their overexpression is indicative of poorer OS [56,57]. These findings reveal that CDGs, owing to their close implication in cancer occurrence and development, may serve as prognostic biomarkers or therapeutic targets.

We also observed that TIME accounts for the difference between the high- and low-risk groups. CD4+ T cells mediate antitumor responses by secreting interferon γ (IFNγ) and tumour necrosis factor (TNF) [58]. The PARP inhibitor olaparib can induce CD8+ T cell infiltration and activate the STING/TBK1/IRF3 pathways, thus inhibiting the growth of triple-negative BRCA [59]. A high level of eosinophils enhances antitumor immunity via direct and indirect mechanisms involving TNF receptor, CC-chemokine receptor 3, vasculature, and interferon-γ receptor [60]. The level of NK cells in the blood has been used to detect metastatic potential in different phenotypes of solid and haematological malignancies [61]. In the present study, consistent relationships between the levels of immune cells (especially central memory CD4 + T cells) and risk scores were observed in different datasets. Earlier research has also indicated that the percentage of central memory CD4+ T cells increases in BRCA-free lymph nodes, providing evidence that these cells might play an inhibitory role in tumour progression and invasion [62].

Similarly, we further revealed that the risk score was negatively correlated with the expression levels of 12 immuno-oncology targets, such as CTLA4, PDCD1, and TNF, which is consistent with the results of previous studies. The expression levels of PD-1

and CTLA4 vary in different cancers and may predict the OS of patients with BRCA and neck squamous cell carcinoma [63]. GZMB is highly expressed in gastric cancer, making it a potential prognostic biomarker [64]. High expression of CD8A, combined with low expression of TAM-specific LOXL4, could predict better OS in hepatocellular carcinoma patients [65]. PD1 expression is closely related to the number of CD8+ T cells in some cancers and the overall response rate following anti-PD1 monotherapy [66]. Therefore, the risk of BRCA may be associated with the expression of immuno-oncological genes and the concentration of immune cells.

We also found that the mutation rates of the CDGs were significantly different between the two groups. Seven genes, TP53, PIK3CA, TTN, and GATA3, were mutated more frequently in the high-risk group. TP53 mutations, usually resulting from chromosomal instability, are involved in oncogene amplification and tumour suppressor gene deletion [67]. TP53 can also initiate the progression of high-grade serous ovarian cancers and basal-like BRCAs [68]. PIK3CA mutation confers poor prognosis and chemo-resistance to HR+ and HER2- BRCA by activating the PI3K pathway [69]. We also found lower mutation rates for five genes in the low-risk subgroup: PIK3CA, TP53, CDH1, TTN, and MUC4. PIK3CA mutations in triple-negative BRCA predict a better outcome [70]. Therefore, mutations in these genes may help clinicians to assess the prognosis of patients with BRCA.

Subsequently, GO analysis revealed that the differentially expressed CDGs were enriched in cytokine-mediated signalling pathways, regulation of system processes, and regulation of lipid metabolic processes. KEGG analysis showed that they were also enriched in pathways associated with malignancy, including striated muscle contraction, vitamin B12 metabolism, and the PID REG GR pathway. ZIP13 activates the Src/FAK pathway to accelerate the pro-metastatic process and downregulate the expression of tumour suppressor genes in ovarian cancer by regulating the cytokine-mediated signalling pathway [71]. The expression levels of lipid metabolism-related factors are upregulated by EGLN1/3, c-Myc, and lymphoid-specific helicase (LSH) to promote the development of lung cancer [72]. GSVA analysis revealed that several pathways were differentially enriched between the high- and low-risk groups. The Notch, JAK-STAT, and B-cell receptor signalling pathways were more enriched in the low-risk group. The Notch signalling pathway plays multiple roles in cancers by regulating angiogenesis, tumor immunity and cancer stemness [73]. The JAK/STAT signalling pathway, regulated by receptor tyrosine kinases, mediates the interaction between BRCA and stromal cells during the progression and metastasis of BRCA [74]. B-cell receptor signalling is active in the TME of solid tumours such as pancreatic cancer [75].

In this study, we verified the potential therapeutic value of CDGs in BRCA. In BRCA patients with lower expression levels of CDGs (NFKBIA and AIFM1), the IC50 increased, but the sensitivity was higher for some targeted drugs, including lifirafenib, dabrafenib, and PLX8394. Lifirafenib (BGB−283), a novel RAF and EGFR inhibitor, can inhibit B-RAFV600-mutated solid tumours [76]. The combination of dabrafenib (BRAF inhibitor) and trametinib (MEK inhibitor) has robust clinical efficacy against BRAF V600E-mutated anaplastic thyroid cancer [77]. PLX8394 represses ERK signalling by specifically disrupting BRAF dimers and RAS-independent BRAF-mutant-driven signalling to kill cancer cells [78]. These studies revealed that targeted therapy might exert a counteractive effect against tumour cells by mediating the expression of CDGs.

Five CDGs were used to construct a prognostic nomogram for BRCA in TCGA cohort. Similarly, a nomogram was established based on the m6A-LPS to predict the OS of lower-grade glioma patients, and the AUC values for 1-, 3-, and 5-year OS were 0.899, 0.860, and 0.806, respectively [79]. Comparatively, our nomogram also had a robust ability to predict the survival rate of BRCA patients.

Distinguishing this study from previous similar works, our research implemented an intricate and innovative bioinformatics analysis on a significantly larger dataset, enhancing the reliability and validity of our findings. We also validated the role of NFKBIA in BRCA development explicitly through cellular experiments, providing a more solid and direct evidence for its regulatory role in BRCA. Additionally, the comprehensive exploration of CDGs in our research brought light to their potential as both prognostic biomarkers and therapeutic targets, a perspective not fully covered in prior research. This extensive analysis, encompassing risk scores, correlation with immune cell levels, mutation rates, and drug sensitivity, further augmented the depth of our study, making it a valuable contribution to the existing literature.

Our study also has several limitations. First, we only explored the role of CDGs in predicting the prognosis of BRCA at the mRNA level; the underlying mechanisms of CDGs require further exploration. Additionally, we discovered a correlation between drug sensitivity and CDG expression, but how the CDGs regulate drug sensitivity was not answered due to the lack of sufficient clinical data.

5. Conclusions

In conclusion, we constructed a five-CDG nomogram with a robust prognostic ability for BRCA. Then, we systematically assessed the expression of CDGs in the TIME, their regulatory mechanisms, and their therapeutic value in BRCA. We also confirmed that NFKBIA suppresses the proliferation and migration of BRCA cells through cellular experiments in vitro. Our study suggests that CDGs may be employed to design more personalized immune and targeted therapies for BRCA.

Ethics statement

This study was approved by the Ethics Committee of the First Affiliated Hospital of Nanjing Medical University, and written informed consent was obtained from the participants (Approval No. IACUC 2107052).

Funding

Code availability

All statistical analyses were performed using R software (version 4.0.1). All patients were randomly divided into training and testing sets using the "caret" R package (https://CRAN.R-project.org/package=corrplot). The coefficients of the five CDGs were obtained via cross-validation using the R package "glmnet." The "limma" R package was used to identify DEGs between the two risk groups. The mutation rate was visualized using R package "maftools." The R packages "ggplot2″, "clusterProfiler", "GOplot, and "enrichplot" were used to obtain enrichment results in the GO and KEGG analyses. ssGSEA was performed using R package "gsva." The "estimate" R package's output was used to investigate the differences in the levels of immune cells between the two groups. The interaction between immuno-oncological targets and CDGs was depicted using the R package "corrplot." The R package "pRRophetic" was used to predict the drug sensitivity. Then, univariate and multivariate Cox proportional regression analyses were conducted on the "Survival" and "Survminer" (https://CRAN.R-project.org/package=survminer) R packages. A heat map was generated using the "pheatmap" R package (https://CRAN.R-project.org/package=pheatmap). The "rms" R package was used to construct the nomograms. The "pROC" R package [52] was used to quantify the AUC values.

Data availability statement

1. Sharing research data helps other researchers evaluate your findings, build on your work and to increase trust in your article. We encourage all our authors to make as much of their data publicly available as reasonably possible. Please note that your response to the following questions regarding the public data availability and the reasons for potentially not making data available will be available alongside your article upon publication. Has data associated with your study been deposited into a publicly available repository? — No.

2. Please select why. — Data included in article/supp. material/referenced in article.

CRediT authorship contribution statement

Xiaoyue Shi: Writing – review & editing, Writing – original draft, Visualization, Validation. **Hao Ding:** Software, Investigation, Formal analysis. **Jing Tao:** Resources, Data curation. **Yanhui Zhu:** Software, Methodology, Data curation. **Xiaoqiang Zhang:** Software, Resources, Data curation. **Gao He:** Software, Resources, Data curation. **Junzhe Yang:** Validation, Methodology, Investigation. **Xian Wu:** Validation, Methodology. **Xiaoan Liu:** Supervision, Resources, Funding acquisition, Conceptualization. **Xiafei Yu:** Supervision, Resources, Project administration, Conceptualization.

Declaration of competing interest

The authors declare that they have no known competing financial interests or personal relationships that could have appeared to influence the work reported in this paper.

Acknowledgements

Appendix A. Supplementary data

Supplementary data to this article can be found online at https://doi.org/10.1016/j.heliyon.2023.e21341.

References

[1] H. Sung, J. Ferlay, R.L. Siegel, M. Laversanne, I. Soerjomataram, A. Jemal, et al., Global cancer statistics 2020: GLOBOCAN estimates of incidence and mortality worldwide for 36 cancers in 185 countries, CA Cancer J Clin 71 (3) (2021) 209–249, https://doi.org/10.3322/caac.21660.

[2] S. Bekeschus, F. SaadatiS. Emmert, The potential of gas plasma technology for targeting breast cancer, Clin. Transl. Med. 12 (8) (2022), e1022, https://doi.org/10.1002/ctm2.1022.

[3] X. Yang, L. Gao, Y. Wei, B. Tan, Y. Wu, C. Yi, et al., Photothermal hydrogel platform for prevention of post-surgical tumor recurrence and improving breast reconstruction, J Nanobiotechnology 19 (1) (2021) 307, https://doi.org/10.1186/s12951-021-01041-w.

[4] R.L. Siegel, K.D. Miller, H.E. FuchsA. Jemal, Cancer statistics, 2021, CA Cancer J Clin 71 (1) (2021) 7–33, https://doi.org/10.3322/caac.21654.

[5] A.G. WaksE, P. Winer, Breast cancer treatment: a review, JAMA 321 (3) (2019) 288–300, https://doi.org/10.1001/jama.2018.19323.

[6] F. Shao, Z. Pan, Y. Long, Z. Zhu, K. Wang, H. Ji, et al., Nectin-4-targeted immunoSPECT/CT imaging and photothermal therapy of triple-negative breast cancer, J Nanobiotechnology 20 (1) (2022) 243, https://doi.org/10.1186/s12951-022-01444-3.

[7] Y. Liang, H. Zhang, X. SongQ. Yang, Metastatic heterogeneity of breast cancer: molecular mechanism and potential therapeutic targets, Semin. Cancer Biol. 60 (2020) 14–27, https://doi.org/10.1016/j.semcancer.2019.08.012.

[8] M. Riegman, M.S. BradburyM. Overholtzer, Population dynamics in cell death: mechanisms of propagation, Trends Cancer 5 (9) (2019) 558–568, https://doi.org/10.1016/j.trecan.2019.07.008.

[9] A. StrasserD, L. Vaux, Cell death in the origin and treatment of cancer, Mol Cell 78 (6) (2020) 1045–1054, https://doi.org/10.1016/j.molcel.2020.05.014.

[10] V. Gadiyar, K.C. Lahey, D. Calianese, C. Devoe, D. Mehta, K. Bono, et al., Cell death in the tumor microenvironment: implications for cancer immunotherapy, Cells 9 (10) (2020), https://doi.org/10.3390/cells9102207.

[11] M. Noguchi, N. Hirata, T. Tanaka, F. Suizu, H. NakajimaJ, A. Chiorini, Autophagy as a modulator of cell death machinery, Cell Death Dis. 11 (7) (2020) 517, https://doi.org/10.1038/s41419-020-2724-5.

[12] Y.S. Abd El-Aziz, P.J. JanssonS. Sahni, Autophagy: a promising target for triple negative breast cancers, Pharmacol. Res. 175 (2022), 106006, https://doi.org/10.1016/j.phrs.2021.106006.

[13] U.M. Parmar, M.P. Jalgaonkar, Y.A. KulkarniM, J. Oza, Autophagy-nutrient sensing pathways in diabetic complications, Pharmacol. Res. 184 (2022), 106408, https://doi.org/10.1016/j.phrs.2022.106408.

[14] G. Marino, M. Niso-Santano, E.H. BaehreckeG. Kroemer, Self-consumption: the interplay of autophagy and apoptosis, Nat. Rev. Mol. Cell Biol. 15 (2) (2014) 81–94, https://doi.org/10.1038/nrm3735.

[15] C. HeD, J. Klionsky, Regulation mechanisms and signaling pathways of autophagy, Annu. Rev. Genet. 43 (2009) 67–93, https://doi.org/10.1146/annurev-genet-102808-114910.

[16] R. JanG, E. Chaudhry, Understanding apoptosis and apoptotic pathways targeted cancer therapeutics, Adv Pharm Bull 9 (2) (2019) 205–218, https://doi.org/10.15171/apb.2019.024.

[17] M. Sauler, I.S. BazanP, J. Lee, Cell death in the lung: the apoptosis-necroptosis Axis, Annu. Rev. Physiol. 81 (2019) 375–402, https://doi.org/10.1146/annurev-physiol-020518-114320.

[18] H. Samaratunga, B. Delahunt, J.R. Srigley, D.M. Berney, L. Cheng, A. Evans, et al., Granular necrosis: a distinctive form of cell death in malignant tumours, Pathology 52 (5) (2020) 507–514, https://doi.org/10.1016/j.pathol.2020.06.002.

[19] W. Tonnus, C. Meyer, A. Paliege, A. Belavgeni, A. von Massenhausen, S.R. Bornstein, et al., The pathological features of regulated necrosis, J. Pathol. 247 (5) (2019) 697–707, https://doi.org/10.1002/path.5248.

[20] M.N. Messmer, A.G. SnyderA. Oberst, Comparing the effects of different cell death programs in tumor progression and immunotherapy, Cell Death Differ. 26 (1) (2019) 115–129, https://doi.org/10.1038/s41418-018-0214-4.

[21] Q. Chen, J. KangC. Fu, The independence of and associations among apoptosis, autophagy, and necrosis, Signal Transduct Target Ther 3 (2018) 18, https://doi.org/10.1038/s41392-018-0018-5.

[22] L. Poillet-PerezE. White, Role of tumor and host autophagy in cancer metabolism, Genes Dev. 33 (11–12) (2019) 610–619, https://doi.org/10.1101/gad.325514.119.

[23] F. Nazio, M. Bordi, V. Cianfanelli, F. LocatelliF. Cecconi, Autophagy and cancer stem cells: molecular mechanisms and therapeutic applications, Cell Death Differ. 26 (4) (2019) 690–702, https://doi.org/10.1038/s41418-019-0292-y.

[24] T. Huang, X. Wan, A.A. Alvarez, C.D. James, X. Song, Y. Yang, et al., MIR93 (microRNA -93) regulates tumorigenicity and therapy response of glioblastoma by targeting autophagy, Autophagy 15 (6) (2019) 1100–1111, https://doi.org/10.1080/15548627.2019.1569947.

[25] H. Zhang, Y. Zhang, X. Zhu, C. Chen, C. Zhang, Y. Xia, et al., DEAD box protein 5 inhibits liver tumorigenesis by stimulating autophagy via interaction with p62/SQSTM1, Hepatology 69 (3) (2019) 1046–1063, https://doi.org/10.1002/hep.30300.

[26] M. Piffoux, E. EriauP, A. Cassier, Autophagy as a therapeutic target in pancreatic cancer, Br. J. Cancer 124 (2) (2021) 333–344, https://doi.org/10.1038/s41416-020-01039-5.

[27] H. Perez-Montoyo, Therapeutic potential of autophagy modulation in cholangiocarcinoma, Cells 9 (3) (2020), https://doi.org/10.3390/cells9030614.

[28] S. Valiyari, M. SalimiS. Bouzari, Novel fusion protein NGR-sIL-24 for targetedly suppressing cancer cell growth via apoptosis, Cell Biol. Toxicol. 36 (2) (2020) 179–193, https://doi.org/10.1007/s10565-020-09519-3.

[29] L. Emdad, P. Bhoopathi, S. Talukdar, A.K. Pradhan, D. Sarkar, X.Y. Wang, et al., Recent insights into apoptosis and toxic autophagy: the roles of MDA-7/IL-24, a multidimensional anti-cancer therapeutic, Semin. Cancer Biol. 66 (2020) 140–154, https://doi.org/10.1016/j.semcancer.2019.07.013.

[30] H. Lu, S. Zhang, J. Wu, M. Chen, M.C. Cai, Y. Fu, et al., Molecular targeted therapies elicit concurrent apoptotic and GSDME-dependent pyroptotic tumor cell death, Clin. Cancer Res. 24 (23) (2018) 6066–6077, https://doi.org/10.1158/1078-0432.CCR-18-1478.

[31] S.M. Wani, A. Gani, S.A. Mir, F.A. MasoodiF, A. Khanday, beta-Glucan: a dual regulator of apoptosis and cell proliferation, Int. J. Biol. Macromol. 182 (2021) 1229–1237, https://doi.org/10.1016/j.ijbiomac.2021.05.065.

[32] S.Y. Lee, M.K. Ju, H.M. Jeon, E.K. Jeong, Y.J. Lee, C.H. Kim, et al., Regulation of tumor progression by programmed necrosis, Oxid. Med. Cell. Longev. 2018 (2018), 3537471, https://doi.org/10.1155/2018/3537471.

[33] A. Karsch-Bluman, A. Feiglin, E. Arbib, T. Stern, H. Shoval, O. Schwob, et al., Tissue necrosis and its role in cancer progression, Oncogene 38 (11) (2019) 1920–1935, https://doi.org/10.1038/s41388-018-0555-y.

[34] S.V. Schmidt, S. Seibert, B. Walch-Ruckheim, B. Vicinus, E.M. Kamionka, J. Pahne-Zeppenfeld, et al., RIPK3 expression in cervical cancer cells is required for PolyIC-induced necroptosis, IL-1 alpha release, and efficient paracrine dendritic cell activation, Oncotarget 6 (11) (2015) 8635–8647, https://doi.org/10.18632/oncotarget.3249.

[35] B. Arneth, Tumor microenvironment, Medicina (Kaunas). 56 (1) (2019), https://doi.org/10.3390/medicina56010015.

[36] Y. Wang, F. Gao, X. Li, G. Niu, Y. Yang, H. Li, et al., Tumor microenvironment-responsive fenton nanocatalysts for intensified anticancer treatment, J Nanobiotechnology 20 (1) (2022) 69, https://doi.org/10.1186/s12951-022-01278-z.

[37] X. Li, X. Geng, Z. ChenZ. Yuan, Recent advances in glioma microenvironment-response nanoplatforms for phototherapy and sonotherapy, Pharmacol. Res. 179 (2022), 106218, https://doi.org/10.1016/j.phrs.2022.106218.

[38] S. Dong, L. ZhengT. Jiang, Loss of lactate/proton monocarboxylate transporter 4 induces ferroptosis via the AMPK/ACC pathway and inhibition of autophagy on human bladder cancer 5637 cell line, J Oncol 2023 (2023), 2830306, https://doi.org/10.1155/2023/2830306.

[39] J. Cai, Y. Hu, Z. Ye, L. Ye, L. Gao, Y. Wang, et al., Immunogenic cell death-related risk signature predicts prognosis and characterizes the tumour microenvironment in lower-grade glioma, Front. Immunol. 13 (2022), 1011757, https://doi.org/10.3389/fimmu.2022.1011757.

[40] S. EngebretsenJ. Bohlin, Statistical predictions with glmnet, Clin Epigenetics 11 (1) (2019) 123, https://doi.org/10.1186/s13148-019-0730-1.

[41] M.E. Ritchie, B. Phipson, D. Wu, Y. Hu, C.W. Law, W. Shi, et al., Limma powers differential expression analyses for RNA-sequencing and microarray studies, Nucleic Acids Res. 43 (7) (2015) e47, https://doi.org/10.1093/nar/gkv007.

[42] S. Hanzelmann, R. CasteloJ. Guinney, GSVA: gene set variation analysis for microarray and RNA-seq data, BMC Bioinf. 14 (2013) 7, https://doi.org/10.1186/1471-2105-14-7.

[43] A. Mayakonda, D.C. Lin, Y. Assenov, C. PlassH, P. Koeffler, Maftools: efficient and comprehensive analysis of somatic variants in cancer, Genome Res. 28 (11) (2018) 1747–1756, https://doi.org/10.1101/gr.239244.118.

[44] M.Y. Zhang, C. Huo, J.Y. Liu, Z.E. Shi, W.D. Zhang, J.J. Qu, et al., Identification of a five autophagy subtype-related gene expression pattern for improving the prognosis of lung adenocarcinoma, Front. Cell Dev. Biol. 9 (2021), 756911, https://doi.org/10.3389/fcell.2021.756911.

[45] G. Yu, L.G. Wang, Y. HanQ, Y. He, clusterProfiler: an R package for comparing biological themes among gene clusters, OMICS 16 (5) (2012) 284–287, https://doi.org/10.1089/omi.2011.0118.

[46] W. Walter, F. Sanchez-CaboM. Ricote, GOplot: an R package for visually combining expression data with functional analysis, Bioinformatics 31 (17) (2015) 2912–2914, https://doi.org/10.1093/bioinformatics/btv300.

[47] Q. Xu, H. Xu, R. Deng, Z. Wang, N. Li, Z. Qi, et al., Multi-omics analysis reveals prognostic value of tumor mutation burden in hepatocellular carcinoma, Cancer Cell Int. 21 (1) (2021) 342, https://doi.org/10.1186/s12935-021-02049-w.

[48] K. Yoshihara, M. Shahmoradgoli, E. Martinez, R. Vegesna, H. Kim, W. Torres-Garcia, et al., Inferring tumour purity and stromal and immune cell admixture from expression data, Nat. Commun. 4 (2013) 2612, https://doi.org/10.1038/ncomms3612.

[49] D. Yang, W. Lyu, Z. Hu, J. Gao, Z. Zheng, W. Wang, et al., Probiotic effects of lactobacillus fermentum ZJUIDS06 and lactobacillus plantarum ZY08 on hypercholesteremic golden hamsters, Front. Nutr. 8 (2021), 705763, https://doi.org/10.3389/fnut.2021.705763.

[50] P. Geeleher, N. CoxR, S. Huang, pRRophetic: an R package for prediction of clinical chemotherapeutic response from tumor gene expression levels, PLoS One 9 (9) (2014), e107468, https://doi.org/10.1371/journal.pone.0107468.

[51] J.A. Zhang, X.Y. Zhou, D. Huang, C. Luan, H. Gu, M. Ju, et al., Development of an immune-related gene signature for prognosis in melanoma, Front. Oncol. 10 (2020), 602555, https://doi.org/10.3389/fonc.2020.602555.

[52] X. Robin, N. Turck, A. Hainard, N. Tiberti, F. Lisacek, J.C. Sanchez, et al., pROC: an open-source package for R and S+ to analyze and compare ROC curves, BMC Bioinf. 12 (2011) 77, https://doi.org/10.1186/1471-2105-12-77.

[53] J. Lu, Y.H. Wang, X.Y. Huang, J.W. Xie, J.B. Wang, J.X. Lin, et al., circ-CEP85L suppresses the proliferation and invasion of gastric cancer by regulating NFKBIA expression via miR-942-5p, J. Cell. Physiol. 235 (9) (2020) 6287–6299, https://doi.org/10.1002/jcp.29556.

[54] A. Van Keymeulen, M.Y. Lee, M. Ousset, S. Brohee, S. Rorive, R.R. Giraddi, et al., Reactivation of multipotency by oncogenic PIK3CA induces breast tumour heterogeneity, Nature 525 (7567) (2015) 119–123, https://doi.org/10.1038/nature14665.

[55] Y. Zhang, Y. Yang, R. Liu, Y. Meng, G. TianQ. Cao, Downregulation of microRNA-425-5p suppresses cervical cancer tumorigenesis by targeting AIFM1, Exp. Ther. Med. 17 (5) (2019) 4032–4038, https://doi.org/10.3892/etm.2019.7408.

[56] J. Qiu, M. Sun, Y. WangB. Chen, Identification and validation of an individualized autophagy-clinical prognostic index in gastric cancer patients, Cancer Cell Int. 20 (2020) 178, https://doi.org/10.1186/s12935-020-01267-y.

[57] J. Lai, B. Chen, H. Mok, G. Zhang, C. RenN. Liao, Comprehensive analysis of autophagy-related prognostic genes in breast cancer, J. Cell Mol. Med. 24 (16) (2020) 9145–9153, https://doi.org/10.1111/jcmm.15551.

[58] A.M. van der Leun, D.S. ThommenT, N. Schumacher, CD8(+) T cell states in human cancer: insights from single-cell analysis, Nat. Rev. Cancer 20 (4) (2020) 218–232, https://doi.org/10.1038/s41568-019-0235-4.

[59] C. Pantelidou, O. Sonzogni, M. De Oliveria Taveira, A.K. Mehta, A. Kothari, D. Wang, et al., PARP inhibitor efficacy depends on CD8(+) T-cell recruitment via intratumoral STING pathway activation in BRCA-deficient models of triple-negative breast cancer, Cancer Discov. 9 (6) (2019) 722–737, https://doi.org/10.1158/2159-8290.CD-18-1218.

[60] S. Grisaru-Tal, M. Itan, A.D. KlionA. Munitz, A new dawn for eosinophils in the tumour microenvironment, Nat. Rev. Cancer 20 (10) (2020) 594–607, https://doi.org/10.1038/s41568-020-0283-9.

[61] N.D. Huntington, J. CursonsJ. Rautela, The cancer-natural killer cell immunity cycle, Nat. Rev. Cancer 20 (8) (2020) 437–454, https://doi.org/10.1038/s41568-020-0272-z.

[62] Y. Vahidi, Z. Faghih, A.R. Talei, M. DoroudchiA. Ghaderi, Memory CD4(+) T cell subsets in tumor draining lymph nodes of breast cancer patients: a focus on T stem cell memory cells, Cell. Oncol. 41 (1) (2018) 1–11, https://doi.org/10.1007/s13402-017-0352-6.

[63] J.N. Liu, X.S. Kong, T. Huang, R. Wang, W. LiQ, F. Chen, Clinical implications of aberrant PD-1 and CTLA4 expression for cancer immunity and prognosis: a pan-cancer study, Front. Immunol. 11 (2020) 2048, https://doi.org/10.3389/fimmu.2020.02048.

[64] J.H. Cheong, H.K. Yang, H. Kim, W.H. Kim, Y.W. Kim, M.C. Kook, et al., Predictive test for chemotherapy response in resectable gastric cancer: a multi-cohort, retrospective analysis, Lancet Oncol. 19 (5) (2018) 629–638, https://doi.org/10.1016/S1470-2045(18)30108-6.

[65] H.Y. Tan, N. Wang, C. Zhang, Y.T. Chan, M. F, YuenY. Feng, Lysyl oxidase-like 4 fosters an immunosuppressive microenvironment during hepatocarcinogenesis, Hepatology 73 (6) (2021) 2326–2341, https://doi.org/10.1002/hep.31600.

[66] L. Pare, T. Pascual, E. Segui, C. Teixido, M. Gonzalez-Cao, P. Galvan, et al., Association between PD1 mRNA and response to anti-PD1 monotherapy across multiple cancer types, Ann. Oncol. 29 (10) (2018) 2121–2128, https://doi.org/10.1093/annonc/mdy335.

[67] L.A. Donehower, T. Soussi, A. Korkut, Y. Liu, A. Schultz, M. Cardenas, et al., Integrated analysis of TP53 gene and pathway alterations in the cancer genome Atlas, Cell Rep. 28 (5) (2019) 1370–1384 e5, https://doi.org/10.1016/j.celrep.2019.07.001.

[68] L. Silwal-Pandit, A. LangerodA, L. Borresen-Dale, TP53 mutations in breast and ovarian cancer, Cold Spring Harb Perspect Med 7 (1) (2017), https://doi.org/10.1101/cshperspect.a026252.

[69] F. Andre, E.M. Ciruelos, D. Juric, S. Loibl, M. Campone, I.A. Mayer, et al., Alpelisib plus fulvestrant for PIK3CA-mutated, hormone receptor-positive, human epidermal growth factor receptor-2-negative advanced breast cancer: final overall survival results from SOLAR-1, Ann. Oncol. 32 (2) (2021) 208–217, https://doi.org/10.1016/j.annonc.2020.11.011.

[70] F. Mosele, B. Stefanovska, A. Lusque, A. Tran Dien, I. Garberis, N. Droin, et al., Outcome and molecular landscape of patients with PIK3CA-mutated metastatic breast cancer, Ann. Oncol. 31 (3) (2020) 377–386, https://doi.org/10.1016/j.annonc.2019.11.006.

[71] X. Cheng, J. Wang, C. Liu, T. Jiang, N. Yang, D. Liu, et al., Zinc transporter SLC39A13/ZIP13 facilitates the metastasis of human ovarian cancer cells via activating Src/FAK signaling pathway, J. Exp. Clin. Cancer Res. 40 (1) (2021) 199, https://doi.org/10.1186/s13046-021-01999-3.

[72] D. LiY. Li, The interaction between ferroptosis and lipid metabolism in cancer, Signal Transduct Target Ther 5 (1) (2020) 108, https://doi.org/10.1038/s41392-020-00216-5.

[73] S. Majumder, J.S. Crabtree, T.E. Golde, L.M. Minter, B.A. OsborneL. Miele, Targeting Notch in oncology: the path forward, Nat. Rev. Drug Discov. 20 (2) (2021) 125–144, https://doi.org/10.1038/s41573-020-00091-3.

[74] R. Butti, S. Das, V.P. Gunasekaran, A.S. Yadav, D. KumarG, C. Kundu, Receptor tyrosine kinases (RTKs) in breast cancer: signaling, therapeutic implications and challenges, Mol. Cancer 17 (1) (2018) 34, https://doi.org/10.1186/s12943-018-0797-x.

[75] J.A. BurgerA. Wiestner, Targeting B cell receptor signalling in cancer: preclinical and clinical advances, Nat. Rev. Cancer 18 (3) (2018) 148–167, https://doi.org/10.1038/nrc.2017.121.

[76] J. Desai, H. Gan, C. Barrow, M. Jameson, V. Atkinson, A. Haydon, et al., Phase I, open-label, dose-escalation/dose-expansion study of lifirafenib (BGB-283), an RAF family kinase inhibitor, in patients with solid tumors, J. Clin. Oncol. 38 (19) (2020) 2140–2150, https://doi.org/10.1200/JCO.19.02654.

[77] V. Subbiah, R.J. Kreitman, Z.A. Wainberg, J.Y. Cho, J.H.M. Schellens, J.C. Soria, et al., Dabrafenib and trametinib treatment in patients with locally advanced or metastatic BRAF V600-mutant anaplastic thyroid cancer, J. Clin. Oncol. 36 (1) (2018) 7–13, https://doi.org/10.1200/JCO.2017.73.6785.

[78] Z. Yao, Y. Gao, W. Su, R. Yaeger, J. Tao, N. Na, et al., RAF inhibitor PLX8394 selectively disrupts BRAF dimers and RAS-independent BRAF-mutant-driven signaling, Nat Med 25 (2) (2019) 284–291, https://doi.org/10.1038/s41591-018-0274-5.

[79] Z. Tu, L. Wu, P. Wang, Q. Hu, C. Tao, K. Li, et al., N6-Methylandenosine-Related lncRNAs are potential biomarkers for predicting the overall survival of lower-grade glioma patients, Front. Cell Dev. Biol. 8 (2020) 642, https://doi.org/10.3389/fcell.2020.00642.